A Rheological Study on the Kinetics of Hybrid Formation in Polypropylene Nanocomposites

Girish Galgali,[†] C. Ramesh,[‡] and Ashish Lele*[,†,§]

Chemical Engineering Division, National Chemical Laboratory, Pune 411 008, India, and Polymer Chemistry Division, National Chemical Laboratory, Pune 411 008, India

Received March 29, 2000

ABSTRACT: We present an experimental investigation on the creep behavior of molten polypropylene organically modified clay nanocomposites. The nanocomposite hybrids were prepared by melt intercalation in an extruder in the presence or absence of a compatibilizer. They were subsequently annealed and simultaneously characterized using high-temperature wide-angle X-ray diffraction and controlled stress rheometry. The creep resistance of compatibilized hybrids was significantly higher than that of uncompatibilized hybrids and also increased with annealing time. The microstructure of the nanocomposites as investigated by TEM and high-temperature WAXD showed the presence of clay crystallites dispersed within the polymer matrix. The creep data together with the microstructural investigation are probably indicative of a small amount of exfoliation from the edges of the clay crystallites during extrusion and annealing. The zero shear viscosity of the compatibilized nanocomposites containing greater than 3 wt % clay was at least 3 orders of magnitude higher than that of matrix resin and the uncompatibilized hybrids. Importantly, the large increase in zero shear viscosity was not accompanied by any increase in the flow activation energy compared to the matrix polymer. The compatibilized hybrids also showed an apparent "yield" behavior. We conclude that the solidlike rheological response of the molten nanocomposite originates from large frictional interactions of the clay crystallites. Compatibilizer has a significant influence in modifying the rheological behavior.

Introduction

Polymer-layered silicate (PLS) nanocomposites exhibit outstanding properties that are synergistically derived from the organic and inorganic components. PLS hybrids exhibit superior mechanical properties,[1] reduced gas permeability,[2] improved solvent resistance,[3] and enhanced ionic conductivity.[4] Such hybrids are also believed to offer unique opportunities for understanding the influence of confined polymers on the properties of macroscopic systems. In general, there are two idealized types of microstructures in PLS nanocomposites, namely, intercalated and exfoliated (or delaminated). In an intercalated hybrid, extended polymer chains reside between the host silicate layers that are typically separated by 1−4 nm (a distance of the order of typical segment length of a polymer chain). Intercalation results in well-ordered multilayered structure with alternating polymer/inorganic layers. In an exfoliated hybrid the silicate layers are randomly dispersed in a continuous polymer matrix such that the interlayer distance is comparable to the radius of gyration of the polymer.[5] Real PLS nanocomposites have a hierarchy of morphologies, which fall in between the two idealized microstructures.[6]

PLS nanocomposites are typically synthesized either by in situ polymerization,[2] i.e., intercalation of a suitable monomer followed by polymerization, or by solution method,[7] i.e., intercalation of dissolved polymer from a solution. For many commercially important nonpolar polymers such as polyolefins, the in situ polymerization or solution techniques cannot be used for preparation of nanocomposites. In such cases, the direct melt intercalation method offers a convenient technique for preparation of hybrids. Melt intercalation involves mixing the layered silicates with the polymer matrix above its softening point.[8] Vaia et al. have studied the kinetics of polystyrene melt intercalation in organically modified mica-type silicates using X-ray diffraction (XRD) and transmission electron microscopy (TEM).[9] They showed that the rate of intercalation is determined by the mass transport of polymer chains into the primary particles of host silicate and is not limited by diffusion inside the silicate galleries.

The structure of PLS nanocomposites is typically elucidated using XRD and TEM.[10] Whereas TEM allows a qualitative understanding of the microstructure through direct visualization, wide-angle X-ray diffraction (WAXD) offers a convenient way to determine the interlayer spacing due to the periodic arrangement of silicate layers in the virgin clay and in intercalated PLS hybrids. However, in the exfoliated or delaminated state where the periodic arrangement is lost, WAXD does not provide definitive information regarding the structure of the nanocomposite. WAXD can also suffer from problems of weak peak intensity, bias toward surface region, and poor peak resolution, particularly in those composites where the clay content is small. Recently, SAXS has been used to probe the superstructure of a delaminated polycaprolactone-layered silicate nanocomposite.[6]

In this work we show that creep measurements in association with WAXD can be used to monitor subtle changes in the microstructure of PLS nanocomposites during the hybrid formation process. We show that creep studies provide a particularly useful analytical technique to understand the origin of the unusual rheological properties of PLS hybrids at a microstruc-

[†] Chemical Engineering Division.
[‡] Polymer Chemistry Division.
[§] Present address: University of Cambridge, Department of Chemical Engineering, Pembroke Street, Cambridge CB2 3RA, UK.
* Corresponding author. e-mail lele@che.ncl.res.in.

10.1021/ma000565f CCC: $20.00
Published on Web 01/18/2001

Table 1. Compositions of the PP−CH Nanocomposites

sample	PP (wt %)	PP−MA (wt %)	clay (wt %)
PPCH1	97	0	3
PPCH2	94	3	3
PPCH5	94	0	6
PPCH6	88	6	6
PPCH8	91	0	9
PPCH9	82	9	9
PPCH25[a]	65	10	25
PPCH26[a]	75	0	25

[a] This composition was specifically used for XRD studies only in order to increase the signal intensity from the clay.

tural level. We report here rheological data of polypropylene−clay hybrids (PPCH), which were prepared by melt compounding polypropylene and commercially available organically modified montmorillonite clay in the presence or absence of a maleic anhydride grafted polypropylene (PP−MA) oligomer as a compatibilizer. The PP−MA oligomer can interact with layers of the clay through strong hydrogen bonding between the polar functional group of PP−MA and the oxygen group of silicates. It has been reported that the intercalated PP−MA hybrid can be easily dispersed in the polypropylene matrix to form nanocomposites, provided the PP−MA is miscible with the polypropylene.[11]

Experimental Section

Materials. Polypropylene (PP, grade Montell KF6100) of MFI = 3 and M_w of approximately 300 000 was used as the matrix phase. Maleic anhydride grafted polypropylene (PP-MA, grade Polybond 3200) of MFI = 140 was used as the compatibilizer. A highly hydrophobic dimethyl dihydrogenated tallow ammonium exchanged montmorillonite clay (DMDHTMC, grade Cloisite 6A) was chosen due to the nonpolar nature of polypropylene. The clay was supplied by Southern Clay Products, Texas. All materials were dried at 80 °C before use.

Preparation of PP−CH. PP and PP−MA were melt blended with DMDHTMC at 175−200 °C in a Bertsoff ZE-25 twin screw extruder having corotating and intermeshing 25 mm screws (L/D = 41.5) at 200 rpm. The residence time inside the extruder was approximately 2.5 min under the processing conditions used in this work. The compositions of the hybrids are shown in Table 1. The extruded strands were pelletized and dried under vacuum at 80 °C for 12 h.

Rheological Characterization of PP−CH. Rheological measurements were performed on as-extruded and annealed samples using a Bohlin CVO-50 controlled stress rheometer fitted with 25 mm diameter parallel plates. Sample disks (1 mm thick and 25 mm diameter) were prepared by compression molding of the extruded pellets at 200 °C for about 3 min. Creep experiments were performed at a small constant shear stress of 10 Pa (for 3% and 6% clay) and 50 Pa (for 9% clay) for a creep time of 180 s at 200 °C. Creep data were collected every 15 min for a period of 3 h during which the sample was annealed in between the parallel plates at 200 °C. In a few creep experiments the stress was gradually increased in a stepwise manner, while in some other experiments creep measurements were done after an initial preshearing of the samples. Low-amplitude oscillatory shear experiments were performed over a frequency range of 0.01−75 Hz on extruded samples as well as on samples annealed between the parallel plates at 200 °C. All experiments were performed under a nitrogen blanket to minimize oxidative degradation of polypropylene.

WAXD. The X-ray diffraction experiments were performed using Rigaku Dmax 2500 diffractometer with Cu target. The system consisted of a rotating anode generator and wide angle powder goniometer fitted with a high-temperature attachment. The generator was operated at 40 kV and 150 mA. The sample holder was a copper block on which a thin film of the sample was formed by melt pressing the as-extruded sample just above its melting temperature. Initially the X-ray hot stage furnace was heated to 200 °C, and then the sample was mounted on the furnace and allowed to equilibrate for 2 min. The temperature was maintained at 200 °C within ±0.5 °C during an annealing period similar to that used during rheological measurements, and the change in the structure was studied by scanning the sample at regular time intervals. Samples were scanned from $2\theta = 1.75°$ to 10° at the scan rate of 8°/min.

Figure 1. TEM image of as-extruded PPCH9 sample at 46 000 magnification.

TEM. The as-extruded pellets were sectioned into roughly 100 nm thin sections at −100 °C using a Reichert Ultracut FC-S ultramicrotome. TEM was done using a Philips 400T machine operating at 100 kV.

Results and Discussion

Microstructure. Figure 1 shows TEM image of the as-extruded PPCH9 sample. It is clear that stacks of silicate layers forming the clay crystallites are dispersed within the polymer matrix. Also, the edges of the crystallites appeared to be better dispersed into the surrounding matrix. Similar images were obtained for other PPCH samples.

Figure 2 shows WAXD patterns for DMDHTMC clay (Figure 2a), PPCH25 (Figure 2b), and PPCH26 (Figure 2c) as a function of annealing time. The clay showed three distinct peaks at $2\theta = 2.2°$, 4.5°, and 7.0° corresponding to the d-spacings of 3.3, 2.0, and 1.0 nm, respectively. On annealing the clay at 200 °C for 30 min, a small shift in the peaks toward the larger 2θ region and a decrease in peak intensities were observed. The right shifts in peaks indicate a decrease in d-spacings, which could be due to slow degradation of the organic modifier at the high annealing temperature. The important point to be noted from the WAXD pattern of DMDHTMC is that the d-spacing of 3.3 nm is already

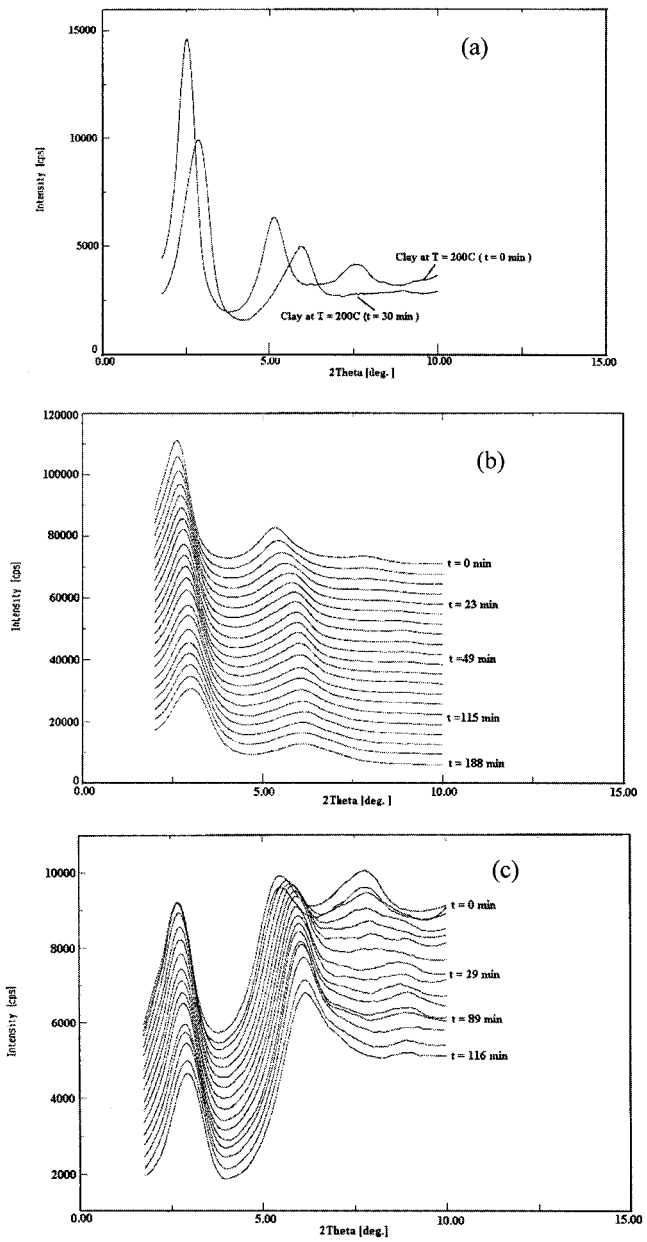

Figure 2. X-ray diffraction data for clay and PPCH samples during in-situ annealing at 200 °C: (a) clay, (b) PPCH25 (in the presence of PP-MA), (c) PPCH26 (in the absence of PP-MA). Annealing times are indicated on the XRD scans.

significantly higher than that of the unmodified Na^+ clay, which has a *d*-spacing of about 1 nm. The larger gallery heights in DMDHTMC are conducive to intercalation of the polymer chains in between the silicate layers provided the interactions between the polymer and the clay are favorable.

The WAXD data for PPCH25 (with compatibilizer) and PPCH26 (without compatibilizer) are shown in parts b and c of Figure 2, respectively, as a function of annealing time. Semicrystalline polypropylene homopolymer does not show any peak in the 2θ region between 1° and 10°. Hence, the peaks in the diffraction pattern are those arising from clay alone. In general, the clay peaks did not shift to lower 2θ region for either of the hybrids, indicating no further increase in *d*-spacings even if intercalation might have occurred. However, a decrease in peak intensity accompanied by a broadening of the peaks was clearly evident in the PPCH25 sample. The increase in intensity with 2θ for the PPCH26 sample was due to background scattering. The WAXD data are in general agreement with the TEM images in that stacks of silicate layers were present in both PPCH samples. WAXD data also suggest that the correlation perpendicular to the silicate layers decreased to a greater extent in the case of PPCH25. This decrease in correlation along the crystallite thickness in PPCH25 could be due to local defects or due to possible exfoliation of a few layers from the end of the stacks into the melt. Finally, it can be said that the WAXD data are indicative of only subtle differences between the morphology of PPCH25 (containing PP−MA) and that of PPCH26 (without PP−MA). However, we will see that the rheological behavior of the PPCH samples with and without compatibilizer showed very large differences and that creep data, in particular, can give valuable information on the time evolution of microstructural changes in the hybrids.

Dynamic Experiments. It has been shown before that end-tethered polymeric nanocomposites show unusual rheological behavior, which is significantly different than that shown by bulk polymers. For example, end-tethered nanocomposites show higher viscosity, greater shear thinning and a distinct nonterminal behavior of the dynamic moduli.[12] Parts a and b of Figure 3 show the time evolution of the elastic and loss moduli, respectively, for PPCH8 and PPCH9 samples, which are subjected to small strain oscillatory shear tests every 10 min during their total annealing duration of 3 h in the rheometer at 200 °C. At high frequencies the elastic modulus of PPCH8 and PPCH9 are almost comparable at similar annealing times and decrease with annealing due to possible degradation of the matrix PP. However, at low frequencies the elastic modulus of PPCH9 are qualitatively different than those of PPCH8. The low-frequency elastic modulus of as-extruded PPCH9 is always higher than that of PPCH8, indicating that the most of the microstructural development in PPCH9 has already occurred during the extrusion process, while only subtle microstructural changes possibly occur during annealing. Further, whereas the elastic modulus of PPCH8 at low frequency decreases with annealing time, that of PPCH9 remains more or less unchanged. Thus, at high frequency the response of the PPCH9 hybrid is dominated by the matrix, while at lower frequencies its solidlike response is strongly influenced by the presence of clay. On the other hand, the low-frequency response of PPCH8 is not dominated by the presence of clay, which highlights the important role played by PP−MA in the formation of the hybrids.

The elastic modulus of PPCH8 showed a near-terminal behavior ($G' \sim \omega^2$), while that of PPCH9 showed a distinct nonterminal behavior similar to that observed for end-tethered nanocomposites.[12] The loss moduli also show similar behavior. The fact that the polypropylene chains are not end-tethered to the silicate layers indicates that nonterminal behavior is a typical property of all PLS nanocomposites. The terminal slopes of the G' data are reported in Table 2 for the different PPCHs and are found to slightly decrease with the clay content above 6 wt % clay in the case of uncompatibilized hybrids and significantly decrease above 3 wt % clay in the case of compatibilized hybrids. Interestingly, the low-frequency plateau in elastic modulus of annealed PPCH9 samples bears similarity with the data for confined polymer melts,[13] indicating that the nonterminal region might be a signature of confined melts.

Table 2. Terminal Slopes of G' vs ω for PP−CH Hybrid

sample	time (h)	terminal slope
PP	0	1.4076
	3	1.4501
PP + 3% clay	0	1.2803
	3	1.0304
PP+ 3% clay + 3% PPMA	0	1.1890
	3	1.3040
PP+ 6% clay	0	1.2729
	3	1.2493
PP+ 6% clay + 6% PPMA	0	0.6604
	3	0.4440
PP + 9% clay	0	1.0641
	3	1.0424
PP + 9% clay + 9% PPMA	0	0.4203
	3	0.1882

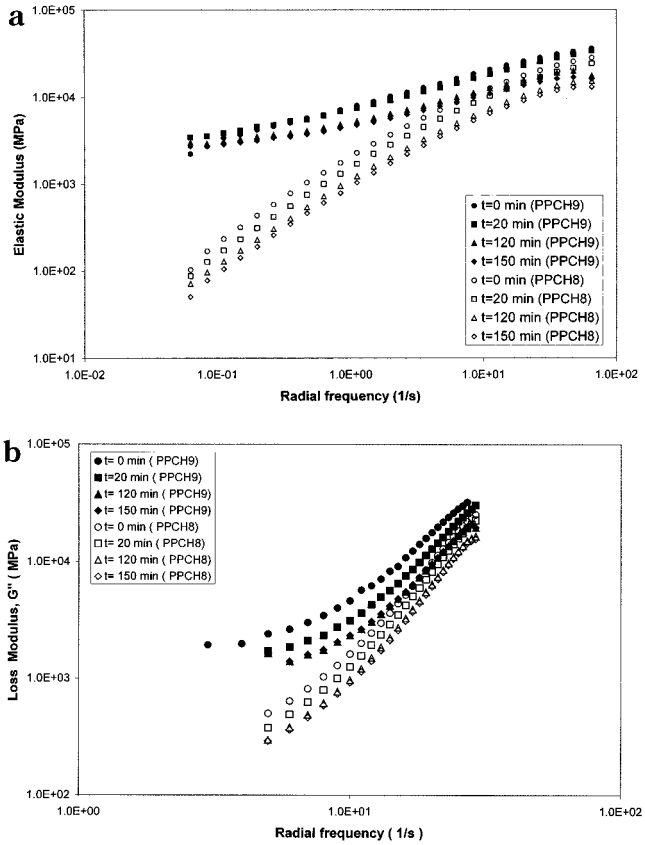

Figure 3. (a) Storage modulus of PPCH8 and PPCH9 samples as a function of annealing time at 200 °C. Unfilled symbols correspond to PPCH8 sample, and filled symbols correspond to PPCH9 sample. (b) Loss modulus of PPCH8 and PPCH9.

However, we will see that this is not the case. In summary, the dynamic data confirm the formation of PP−clay nanocomposites and is indicative of subtle microstructural changes occurring during annealing of the hybrids.

Creep Experiments. Creep experiments are ideally suited for monitoring the solidlike response of materials. Creep data are also important because of its direct relevance to polymer processing and to product performance. In a creep experiment the sample is subjected to a small constant stress, and its deformation is recorded as a function of time. Figure 4 shows the creep behavior of two representative samples, PPCH5 (without compatibilizer) and PPCH6 (with compatibilizer). The extruded samples were annealed in the rheometer at 200 °C, and creep data were recorded every 10 min for a total period of 3 h. The creep compliance of the extruded PPCH6 was considerably lower than that of

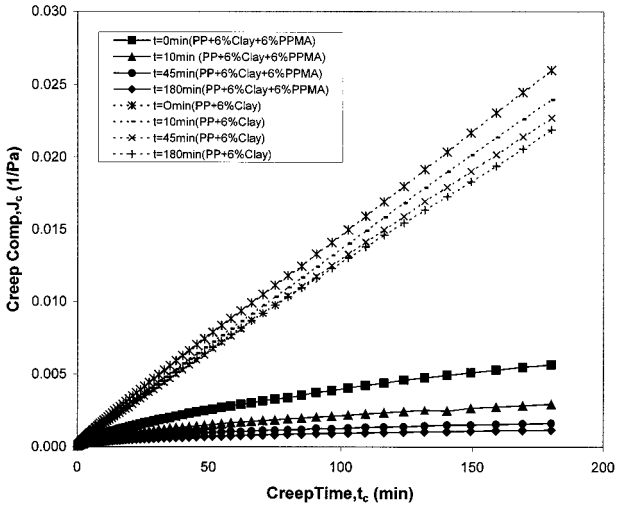

Figure 4. Creep data for PPCH5 and PPCH6 samples. Dotted lines correspond to PPCH5 (absence of PP-MA) sample, while dark lines correspond to PPCH6 (presence of PP-MA) samples.

PPCH5, indicating that a large part of the microstructural changes in PPCH6 had occurred during extrusion. However, the creep compliance of PPCH6 gradually decreased further to a very low (solidlike) value during the annealing period of 3 h, indicating that subtle microstructural changes were still occurring under essentially zero-shear conditions. The continuous variation of creep compliance with time is distinct and easy to measure, thus providing a sensitive method for monitoring the kinetics of microstructural changes during annealing.

Creep data also give valuable information on the zero-shear viscosity, which is shown in Figure 5a for various PPCH samples. There are several interesting features of the viscosity data. While the zero-shear viscosity of polypropylene homopolymer (or of PP/PP−MA blend) decreased continuously with annealing, the viscosity of PPCH samples (in the presence or absence of PP-MA) increased continuously with annealing time. The viscosity of hybrids rose rapidly initially and later saturated at longer times (2−3 h) to a near-constant value. Importantly, the viscosity of compatibilized hybrids was always significantly higher than that of uncompatibilized hybrids. The decrease in the viscosity of PP homopolymer is an indication of its thermal degradation under the experimental conditions, while the increase in viscosity of the PPCH samples is indicative of the microstructural changes occurring during annealing. Further, it was observed that the viscosity of compatibilized hybrids increased sharply after 3 wt % clay loading as shown in Figure 5b, whereas that of uncompatibilized hybrids increased after about 6 wt % clay loading but certainly not as significantly as for the compatibilized hybrids.

There can be two different plausible hypotheses for explaining the observed solidlike behavior of the PP nanocomposites (and indeed of any PLS nanocomposites in general). One hypothesis could be that the solidlike rheological behavior arises from the confinement of polymer chains within the silicate layers. Indeed, it has been reported that the viscosity of confined polymer melts is greater than that of bulk chains.[13,14] The large viscosity of confined melts is believed to arise from an "immobilized hydrodynamic layer" near the wall having a thickness of the order of radius of gyration of the polymer chain.[13] According to a recent scaling model of

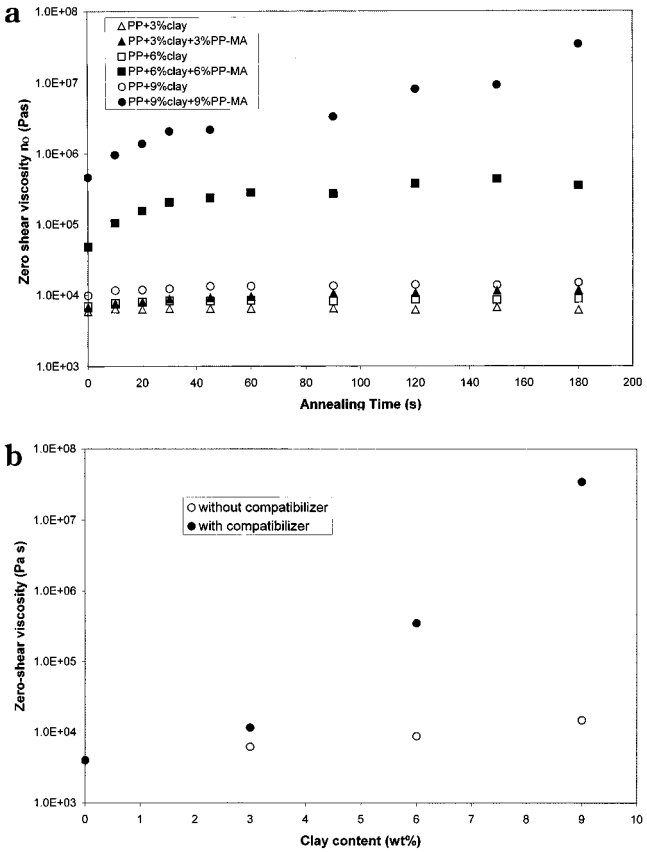

Figure 5. (a) Zero shear viscosity as a function of annealing time for several PPCH samples in the presence (denoted by filled symbols) and absence (denoted by open symbols) of PP-MA. (b) Zero-shear viscosity as a function of clay content for samples with and without compatibilizer.

Semenov and Doi[15] for shear flow of melts confined between parallel plates separated by a distance $h/a \sim N^{1/2}$, where a is the segment length and N is the number of segments in the polymer chain, the relative zero-shear viscosity of the confined melt (η_0^c) with respect to the bulk viscosity (η_0^b) can be given as

$$\frac{\eta_0^c}{\eta_0^b} \sim \frac{a}{h}\frac{\lambda^c}{\lambda^b} \sim \left(\frac{h}{a}\right)^2 \quad \text{for } \lambda^c/\lambda^b \sim (h/a)^3 \qquad (1)$$

Here, λ^c and λ^b are segment relaxation times of the confined and bulk polymer chains, respectively. Thus, the scaling model predicts that if $\lambda^c \gg \lambda^b$ and if the separation distance were of the order of radius of gyration of the polymer chain (as is typically the situation for exfoliated hybrids), then the zero-shear viscosity of the confined system would scale as N, which is typically of the order of 100 in commercial polypropylene resins. Thus, the viscosity of a confined melt can be several times that of the bulk viscosity. The underlying physics for the increased viscosity of confined polymers is the slow relaxation of such chains arising from a larger barrier for segmental motions in the confined space, particularly very close to the boundaries.[16] Hence, if the observed increase in the zero-shear viscosity of polymeric-layered silicate nanocomposites were a signature of the larger barrier for flow of confined chains, then the flow activation energy for nanocomposites should be significantly higher than that for bulk polymer. We have measured the flow activation energy of PPCH compounds from creep data obtained at various

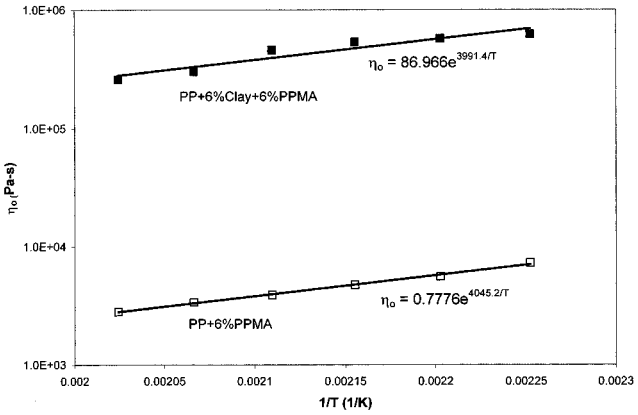

Figure 6. Arrhenius plot of zero shear viscosity as a function of temperature. The activation energy for flow is calculated from the slopes indicated in the figure.

temperatures as shown in Figure 6. It is seen that the activation energy of the PPCH6 sample (~33 kJ/g mol) is nearly the same as that of the PP/PP−MA matrix or of PP homopolymer (~35 kJ/g mol).[17] This indicates that the highest energy barrier for flow in the nanocomposites is the same as that in the bulk polymer, which is in analogy to the finding that the activation energy for diffusion during intercalation was nearly equal to that for self-diffusion in the bulk.[9] This leads to the definitive conclusion that the solidlike rheological response of PLS nanocomposites does not arise from confinement of chains.

An alternative hypothesis for explaining the solidlike rheological behavior of the hybrids is that such a response can arise from frictional interactions between the anisotropic clay crystallites. These interactions can become particularly significant at higher clay contents, i.e., above a percolation limit, which can result in a strong dependence of the viscosity on clay loading. We have indeed observed such dependence in our materials (see Figure 5b).

An important property of filled materials above the percolation limit of filler content is the apparent "yielding" after a critical stress. The so-called yield stress of a material is a useful engineering parameter to describe the flow behavior of several non-Newtonian fluids; however, a true yield stress is a myth since all materials "flow" at all stresses given sufficient time.[18] A yielding fluid typically shows a high Newtonian viscosity at low stresses; i.e., it creeps at low stresses, following which there is a sharp drop in viscosity over a narrow range of higher stresses. This is termed as the yielding behavior. In Figure 7a we show the viscosity of PPCH9 as a function of shear stress. The material creeps at low stresses in a Newtonian manner followed by apparent yielding at about 1000 Pa, in which the viscosity drops by more than 3 orders of magnitude in a very narrow range of shear stress. We have confirmed that the drop in viscosity is not a slip artifact. Slip does occur, however, at much higher stresses, which is not included in the figure. The above data clearly indicate that the large zero-shear viscosity of the material arises from frictional interactions of silicate layers that form a percolating network. At shear stresses greater than the apparent yield stress the structure starts to break down possibly by incipient alignment of the silicate layers along flow direction. This causes the material to flow to increasingly greater extent.

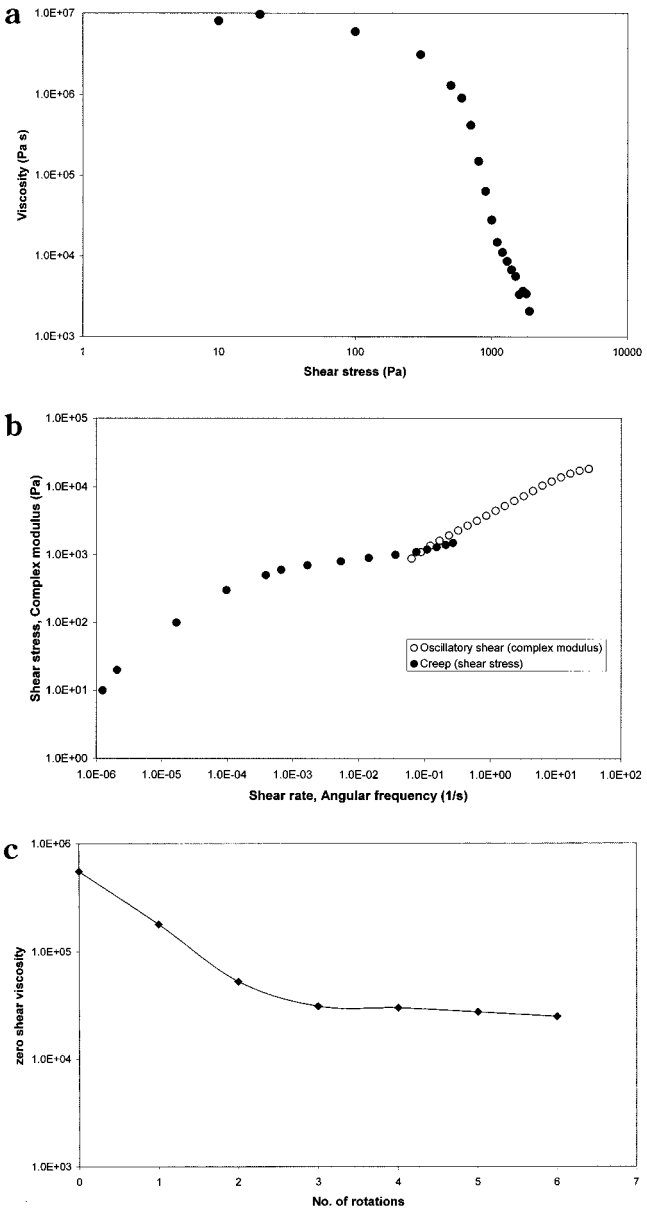

Figure 7. (a) Viscosity of PPCH9 as a function of shearing stress, (b) shear stress and complex modulus of PPCH9 as a function of shear rate and frequency, and (c) zero shear viscosity of PPCH9 as a function of preshear.

Figure 7b shows a combined plot of shear stress vs shear rate and complex modulus vs frequency for PPCH9 sample. The shear rates were measured by creep experiments in which the shear stress was increased in a stepwise manner. The complex modulus was calculated from the dynamic data on the same sample (see Figure 3). At low shear rates a Newtonian response is seen in which the shear rate increased linearly with shear stress. This was followed by a plateau of shear stress (the apparent yield stress) for a wide range of shear rates. Further, the complex modulus matches the yield shear stress value in the low-frequency region, thereby indicating that the nonterminal region in the dynamic data is, in fact, a signature of the yielding phenomenon of PLS nanocomposites.

Finally, Figure 7c shows the effect of shear alignment on the zero-shear viscosity of PPCH9. The zero-shear viscosity was measured by creep experiments after preshearing the sample for a different number of steady shear rotations between the parallel plates. It can be seen that the viscosity decreases steadily with preshearing, which supports the hypothesis of alignment of the clay crystallites in the flow direction. These observations are in a sense similar to the large-amplitude dynamic experimental results of Krishnamoorthi and Giannelis.[12] Thus, the results of various creep experiments presented here clearly indicate that the solidlike rheological response of PPCH compounds (or of PLS nanocomposites in general) arises due to strong frictional interactions between silicate sheets.

During the course of writing this work we have come across the recent results of Ren at al.,[19] who arrive at similar conclusions by carrying out dynamic rheological measurements on intercalated polystyrene−polyisoprene diblock copolymers. However, there are important differences between the present results and their work, which we wish to highlight. First, we have investigated two different hypotheses, namely, the effect of confined melts within clay layers and the effect of frictional interactions between anisotropic clay crystallites, both of which could influence the rheological behavior of PLS nanocomposites. By carrying out creep experiments, we clearly show that the major influence is due to frictional interactions. Second, our data suggest that the presence of a compatibilizer plays a key role in influencing the rheological behavior. While the XRD data indicate that the interlayer spacing between clay sheets is the same for compatibilized and uncompatibilized hybrids, the rheology data show a major difference between the response of compatibilized and uncompatibilized systems to shearing deformations. We believe that this difference arises from a small amount of exfoliation of silicate layers from the edges of the crystallites when a compatibilizer was used. A rough calculation of the average crystal dimension perpendicular to the silicate layers in a PPCH25 sample using the peak widths data of WAXD and the Scherrer formula indicates that the average correlation length decreases from 13 nm before annealing to about 8 nm after annealing for 3 h. This implies that the number of silicate layers decreased from approximately six to four during annealing. No decrease was observed for the uncompatibilized PPCH26 sample. We believe that the exfoliated silicate layers might play a crucial role in effecting the intercrystallite frictional interactions during shearing deformations by "bridging" different crystallites and thus creating a percolating network that resists flow.

It is furthermore informative to note that a similar type of rheological response (yielding and nonterminal behavior) has been observed in diverse macroscopic and microscopic filled systems such as high glass filled polypropylene[20] and aqueous PTFE nanodispersions.[21] The major difference between these materials and PLS nanocomposites is that whereas the former require very high weight percent loading of fillers (typically 40−60 wt % for glass and about 60−70 wt % nanoparticles), the PLS nanocomposites show a solidlike behavior at much lower weight percent loadings (less than 6 wt % in our case). This is mainly due to the finer dispersion of the silicate layers into the matrix and the very high aspect ratio of the silicate layers.

Conclusions

We have shown that polymeric layered silicate nanocomposites show a solidlike rheological response, which include nonterminal dynamic behavior, apparent yielding at higher shearing stresses, and a strong dependence

of viscosity on clay content. The nonterminal dynamic behavior is consistent with the yielding process. The solidlike rheological response is independent of the finer structure of the nanocomposites, i.e., whether they are end-tethered or melt intercalated. We have shown that the typical rheological response of layered silicate nanocomposites arises from frictional interactions between the silicate layers and not due to immobilization of confined polymer chains between the silicate layers. Specifically, the large rise in the viscosity does not arise from a high activation energy barrier, which might be expected for a confined chain. Further, we have shown that the creep behavior is very sensitive to the microstructural changes occurring in the nanocomposite. The creep data together with the XRD suggest that some of the silicate layers from the edges of the crystallites possibly exfoliate into the matrix during annealing of the hybrid. The possibility of exfoliation is greatly enhanced by the presence of a compatibilizer. The exfoliated layers can bridge different silicate crystallites to form a percolating network that strongly resists deformation.

Acknowledgment. This work was funded by the CSIR Young Scientist Award project of one of us (A. K. Lele; Grant P81113YSA). We acknowledge the generous gifts from Southern Clay Products, USA. We are also grateful to Dr. Jeremy Skepper and Dr. Austin Hockaday from the Multi-imaging Centre and Dr. Chris Boothroyd from the Department of Materials Science at the University of Cambridge for helping with the TEM images.

References and Notes

(1) Kojima, M.; Usuki, A.; Okada, A.; Kamigato, O. *J. Mater. Res.* **1993**, *8*, 1185. Messersmith, P. B.; Giannelis, E. P. *Chem. Mater.* **1994**, *6*, 1719. Wang, M. S.; Pinnavaia, T. J. *Chem. Mater.* **1994**, *6*, 468.

(2) Messersmith, P. B.; Giannelis, E. P. *J. Polym. Sci., Part A: Polym. Chem.* **1995**, *33*, 1047.

(3) Brunside, S. D.; Giannelis, E. P. *Chem. Mater.* **1995**, *7*, 1597.

(4) Vaia, R. A.; Vasudevan, S.; Krawiec, W.; Scanlon, L. G.; Giannelis, E. P. *Adv. Mater.* **1995**, *7*, 154.

(5) Giannelis, E. P.; Krishnamoorti, R.; Manias, E. *Adv. Polym. Sci.* **1999**, *138*, 108.

(6) Vaia, R. A.; Lincoln, D. D.; Wang, Z.-G.; Hsiao, B. S. *Polym. Mater. Sci. Eng.* **2000**, *82*, 257.

(7) Wu, J.; Lerner, M. *Chem. Mater.* **1993**, *5*, 835.

(8) Giannelis, E. P. *Adv. Mater.* **1996**, *8*, 29.

(9) Vaia, R. A.; Jandt, K. D.; Kramer, E. J.; Giannelis, E. P. *Macromolecules* **1995**, *28*, 8080.

(10) Kurokawa, Y.; Yasuda, H.; Oyo, A. *J. Mater. Sci., Lett.* **1997**, *16*, 1670. Kurokawa, Y.; Yasuda, H.; Oyo, A. *J. Mater. Sci., Lett.* **1996**, *15*, 1481.

(11) Kawasumi, M.; Hasegawa, N.; Kato, M.; Usuki, A.; Okada, A. *Macromolecules* **1997**, *30*, 6333. Hasegawa, N.; Kawasumi, M.; Kato, M.; Usuki, A.; Okada, A. *J. Appl. Polym. Sci.* **1998**, *67*, 87.

(12) Krishnamoorti, R.; Giannelis, E. P. *Macromolecules* **1997**, *30*, 4097.

(13) Luengos, G.; Schmitt, F.; Hill, R.; Israelachvili, J. *Macromolecules* **1997**, *30*, 2482.

(14) Khare, R.; Pablo, J.; Yethiraj, A. M. *Macromolecules* **1996**, *29*, 7910.

(15) Subbotin, A.; Semenov, A.; Doi, M. *Phys. Rev. E* **1997**, *56*, 623.

(16) Manias, E.; Zax, D. B.; Anastasiadis, S. H. *Polym. Mater. Sci. Eng.* **2000**, *82*, 259.

(17) Barakos, G.; Mitsoulis, E.; Tzoganakis, C. *J. Appl. Polym. Sci.* **1996**, *59*, 543.

(18) Barnes, H. A. J. *Non-Newtonian Fluid. Mech.* **1999**, *81*, 133.

(19) Ren, J.; Silva, A. S.; Krishnamoorti, R. *Macromolecules* **2000**, *33*, 3739.

(20) Yamane, H.; Komoto, S.; Zhang, W.; Takahashi, M. *Proc. XIIIth Int. Congr. Rheol.* **2000**, *4*.

(21) Marchese, E.; Sanguineti, A.; Lapasin, R. *Proc. XIIIth Int. Congr. Rheol.* **2000**, *4*, 166.

MA000565F